



**HAL**  
open science

# Development of fine-tuned top-down mass spectrometry strategies in the chromatographic time scale (LC-TD-MS) for the complete characterization of an anti EGFR single domain antibody-drug conjugate (sdADC)

Rania Benazza, Greg Papadakos, Jen Thom, H el ene Diemer, Graham Cotton, Sarah Cianf erani, Oscar Hernandez Alba

## ► To cite this version:

Rania Benazza, Greg Papadakos, Jen Thom, H el ene Diemer, Graham Cotton, et al.. Development of fine-tuned top-down mass spectrometry strategies in the chromatographic time scale (LC-TD-MS) for the complete characterization of an anti EGFR single domain antibody-drug conjugate (sdADC). 2024. hal-04779656

**HAL Id: hal-04779656**

**<https://hal.science/hal-04779656v1>**

Preprint submitted on 13 Nov 2024

**HAL** is a multi-disciplinary open access archive for the deposit and dissemination of scientific research documents, whether they are published or not. The documents may come from teaching and research institutions in France or abroad, or from public or private research centers.

L'archive ouverte pluridisciplinaire **HAL**, est destin ee au d ep ot et  a la diffusion de documents scientifiques de niveau recherche, publi es ou non,  emanant des  tablissements d'enseignement et de recherche fran ais ou  trangers, des laboratoires publics ou priv es.

1  
2  
3  
4  
5  
6  
7  
8  
9  
10  
11  
12  
13

**Development of fine-tuned top-down mass spectrometry strategies  
in the chromatographic time scale (LC-TD-MS) for the complete  
characterization of an anti EGFR single domain antibody-drug  
conjugate (sdADC)**

**Rania Benazza<sup>1, 2</sup>, Greg Papadakos<sup>3</sup>, Jen Thom<sup>3</sup>, Helene Diemer<sup>1, 2</sup>, Graham Cotton<sup>3</sup>, Sarah  
Cianférani<sup>1, 2</sup> and Oscar Hernandez-Alba<sup>1, 2</sup>**

<sup>1</sup> Laboratoire de Spectrométrie de Masse BioOrganique, IPHC UMR 7178, Université de Strasbourg,  
CNRS, 67087 Strasbourg, France

<sup>2</sup> Infrastructure Nationale de Protéomique ProFI—FR2048, 67087 Strasbourg, France

<sup>3</sup> Almac discovery, Edinburgh Technopole, Milton Bridge, Penicuik, Scotland, EH26 0BE, United  
Kingdom

14 **Abstract:** Even though mAbs have attracted the biggest interest in the development of therapeutic  
15 proteins, next generation of therapeutics such as single-domain antibodies (sdAb) are propelling an  
16 increasing attention as new alternatives with appealing applications in different clinical areas. These  
17 constructs are small therapeutic proteins formed by a variable domain of the heavy chain of an  
18 antibody with multiple therapeutic and production benefits compared to their mAb counterparts.  
19 These proteins can be subjected to different bioconjugation processes to form single-domain antibody-  
20 drug conjugates (sdADC) and hence increase their therapeutic potency, and, akin to other therapeutic  
21 proteins, nanobodies and related products require dedicated analytical strategies to fully characterize  
22 their primary structure prior to their release to the market.

23 In this study we report for the first time on the complete sequence characterization of a conjugated  
24 anti-EGFR 15 kDa sdADC by using cutting-edge top-down mass spectrometry strategies in combination  
25 with liquid chromatography (LC-TD-MS). Mass analysis revealed a highly homogeneous sample with  
26 one conjugated molecule. Subsequently, the reduced sdADC was submitted to different fragmentation  
27 techniques namely higher-energy collisional dissociation (HCD), electron-transfer dissociation (ETD),  
28 and ultraviolet photo-dissociation (UVPD) allowing to unambiguously assess the conjugation site with  
29 16 diagnostic fragment ions and more than 85% of global sequence coverage. The sequence coverage  
30 of the non-reduced protein was significantly lower (around 33%), however the thorough analysis of  
31 the fragmentation spectra and the inclusion of the internal fragments corroborated the presence of  
32 the intra-molecular disulfide bridge along with the localization of the conjugation site.

33 Altogether, our results pinpoint the complementarity of the different fragmentation techniques to  
34 provide a thorough analytical characterization of sdAbs-formats even in the chromatographic time-  
35 scale, which allows a high-throughput and streamlined analysis of this kind of therapeutic proteins  
36 facilitating the implementation on dedicated R&D laboratories.

37

## 38 1. Introduction

39 Monoclonal antibodies (mAbs) have changed the paradigm of cancer treatment over the last decades  
40 with more than 170 approved mAbs world-wide, and more than 200 of mAb biotherapeutics entering  
41 clinical studies per year since 2021.<sup>1</sup> However, in oncology, mAbs can encounter tumor resistance  
42 mechanisms and their large size comprises penetration into solid tumours, limiting therapeutic  
43 efficacy. Thereby, efforts in protein engineering have been focused on the conception of next  
44 generation of biotherapeutics to widen their therapeutic applications. Among these entities, single-  
45 domain antibodies (sdAb), also known as heavy chain variable domain (VHHs) or nanobodies (originally  
46 trademarked in 2003 by Ablynx), have gained increased attention with currently three approved  
47 formats on the market<sup>2</sup> and around 37 nanobody candidates undergoing clinical trials<sup>3</sup> so far.

48 SdAbs derive from the naturally occurring heavy-chain antibodies (HcAbs) in camelids<sup>4</sup>. They are  
49 constituted of four relatively constant framework regions along with the three complementarity-  
50 determining regions (CDRs) responsible for antigen binding. Thereby, nanobodies are substantially  
51 small-sized proteins (~15 kDa) with appealing advantages against their mAb counterparts, *i.e.* better  
52 tissue penetration,<sup>6-9</sup> the possibility to bind clefts and cavities of target antigen,<sup>10-11</sup> exhibit lower  
53 toxicity and immunogenicity,<sup>12-13</sup> enhanced solubility,<sup>14</sup> and stability,<sup>15</sup> and lower structural  
54 heterogeneity. Furthermore, production of sdAbs can be carried out in low-cost systems like *E. coli*<sup>16</sup>  
55 or yeast,<sup>17</sup> reducing the overall production cost. For all these reasons, sdAbs have found their way into  
56 different applications such as infectious diseases,<sup>18</sup> cancer therapy,<sup>19</sup> and central nervous system (CNS)  
57 disorders.<sup>20</sup> Akin to mAbs, nanobodies can be subjected to covalent modifications allowing  
58 incorporation of cargo molecules with different properties allowing the use of conjugated nanobodies  
59 as drug carriers<sup>21</sup> (single domain antibody-drug conjugate, sdADC) or imaging probes.<sup>22</sup> Similar to other  
60 biotherapeutic proteins, the primary structure of sdAbs, and sdADCs has to be thoroughly assessed  
61 prior to their commercialization including sequence assessment, identification of post-translational  
62 modifications, and the precise localization of the position of the cargo molecules (for conjugated  
63 formats) through the development of tailored analytical methods.

64 The development of complementary activation techniques and their subsequent implementation in  
65 last generation high resolution MS platform has paved the way for the development of analytical  
66 workflows envisaging protein sequencing at the intact level, *i.e.*, without any prior enzymatic digestion.  
67 These strategies are encompassed under the term top-down mass spectrometry (TD-MS) and have  
68 been applied to a large variety of biomolecules among which, membrane proteins,<sup>23-26</sup> histones,<sup>27-29</sup>  
69 and oligonucleotides.<sup>30-32</sup> MABs, and derived products such as antibody drug conjugates (ADCs) have  
70 also been subjected to TD-MS studies, mainly due to the advent of complementary fragmentation  
71 techniques. In most of the cases, a limited proteolysis is performed followed by a reduction step to  
72 downsize the mAb-derived protein scaffold,<sup>33-42</sup> and thus mitigating the challenges associated to the  
73 fragmentation of 150 kDa proteins with several chains and multiple inter-, and intra-molecule disulfide  
74 bridges. However, several examples of TD-MS studies of mAbs,<sup>43-50</sup> and ADCs<sup>51-52</sup> can be found in the  
75 literature, illustrating the potential of these methods in the characterization of biotherapeutics at the  
76 intact level. More particularly, Loo and coworkers combined ECD and HCD fragmentation (EChcD) to  
77 perform TD-MS on one mAb and its conjugated ADC under native conditions,<sup>51</sup> reaching an overall  
78 sequence coverage of 70% of both compounds with specific fragment ions allowing the assessment of  
79 intra-molecular disulfide bridges and 58% of payload conjugation sites.

80 Despite the numerous publications showcasing the advantages of TD-MS workflows for intact protein  
81 sequencing, sdAbs and sdADCs have been scarcely characterized using these strategies. In 2010,  
82 Resemann *et al.* performed the *de novo* sequencing of a 13 kDa nanobody using a TD-MS assisted  
83 bottom up (BU) approach.<sup>53</sup> In this case, the fragmentation of the intact nanobody was performed with  
84 MALDI in-source decay matrix assisted laser desorption ionization (MALDI-ISD) with two different  
85 matrix compositions in order to favor fragmentation of both protein termini, and thus provide an  
86 extended protein sequence characterization. A more recent study published by Macias *et al.* applied  
87 ultraviolet photo-dissociation (UVPD) activation to fragment three different nanobody-antigen pairs.<sup>54</sup>  
88 This experiment was conducted under native MS conditions (nMS) with the main purpose of inferring  
89 structural insights onto the quaternary structure of nanobody-antigen pairs from their corresponding  
90 UVPD fragmentation spectra. In this context, the fragmentation of the apo-, and holo- forms of the  
91 nanobodies were compared to detect significant fragmentation differences upon antigen binding.  
92 According to the reported results, the fragment ions originated under both conditions pinpointed a  
93 fragmentation suppression located at the antigen-nanobody interfaces leading to the conclusion that  
94 UVPD-based native TD-MS can significantly contribute to determine nanobody's paratopes.  
95 As evidenced by the scarce number of reported studies, nanobodies, and their conjugated  
96 counterparts have not been extensively studied with TD-MS workflows for their primary structure  
97 characterization. Moreover, both studies used direct infusion without providing further evidence  
98 demonstrating the suitability of the TD-MS strategies in the characterization of sdAbs in the  
99 chromatographic time scale. Here we report for the first time on the characterization of an in-house  
100 sdADC using a tailored reversed-phase liquid chromatography top-down mass spectrometry (RPLC-TD-  
101 MS) strategy based on higher energy collision induced dissociation (HCD), electron transfer  
102 dissociation (ETD), and ultraviolet photo-dissociation (UVPD) techniques. The experimental conditions  
103 of each individual activation technique were optimized to improve the fragmentation yield of the  
104 peptide backbone, highlighting the advantages/limitations of each fragmentation technique in terms  
105 of overall sequence coverage, localization of the conjugation site, and the identification of signature  
106 fragment ions to determine the presence of the intra-molecular disulfide bridge. Overall, this study  
107 provides a complete picture about the suitability of LC-TD-MS strategies in the characterization of the  
108 primary structure of next generation sdAbs, and sdADCs biotherapeutics.

## 109 **2. Material & methods**

### 110 *2.1 Chemicals and reagents*

111 All buffers and the chemicals used for the protein purification and functionalisation were purchased  
112 from Merck. *E. Coli* cells and chitin affinity chromatography resin were purchased from NEB, Luria-  
113 Bertani (LB) media, ampicillin (AMP), isopropyl  $\beta$ -D-1-thiogalactopyranoside (IPTG) were purchased  
114 from MelfordAlexa Fluor™ 488 C5 Maleimide (AF488) was purchased by ThermoFisher and 5 ml HiTrap  
115 desalting columns by Cytiva.

116 All chemicals were purchased from Sigma-Aldrich (France): acetonitrile (ACN), ammonium acetate  
117 (AcNOH<sub>4</sub>), dithiothreitol (DTT) and trifluoroacetic acid (TFA). RapiGest™ reagent was purchased from  
118 Waters (France) and trypsin from Promega (France). All aqueous solutions were prepared with ultra-

119 pure water system (Sartorius, Göttingen, Germany). LockMass and RDa Calibrant solutions used on the  
120 BioAccord were obtained from Waters (Manchester, UK) and the calibration solution used on the  
121 Eclipse was a Pierce FlexMix from Thermo Fisher (France). The anti-EGFR nanobody was prepared at  
122 Almac Discovery (Scotland, UK).

## 123 2.2 Anti-EGFR production, expression, purification and conjugation

124 **sdAb preparation and thiol functionalisation** —The anti-EGFR VHH 7C12 cloned to the N-terminus of  
125 a GyrA intein-chitin binding domain fusion, was expressed in *E. coli* cells and captured on chitin beads  
126 as previously described (cite: <https://pubs.acs.org/doi/10.1021/acsmacrolett.8b00461>).

127 The 7C12 intein fusion protein was then cleaved by overnight incubation at room temperature with  
128 200 mM cysteamine in 200 mM NaCl, 50 mM sodium phosphate buffer, pH 6.9, to generate the  
129 corresponding C-terminal thiol-functionalised 7C12 protein. Cysteamine excess was further eliminated  
130 by size-exclusion chromatography (**Figure S1**).

131 **sdAb conjugation**— To conjugate to the C-terminal thiol group of 7C12 (generated by cysteamine  
132 cleavage of the precursor intein-fusion protein and referred to as the C-terminal cysteamine thiol), the  
133 purified protein was incubated with a 4-fold molar excess of Alexa Fluor 488 maleimide dye at room  
134 temperature for 1h. ..The excess dye was removed using a 5 ml HiTrap desalting column equilibrated  
135 in PBS, pH 7.4. , The labelling was confirmed by SDS-PAGE and and ESI-TOF MS (Bruker Daltonics) The  
136 protein concentration and the degree of labelling were calculated according to the AF488  
137 ThermoFisher manual using the molar extinction coefficient of the protein.

## 138 2.3 SEC-nMS analysis

139 Size exclusion chromatography coupled to mass spectrometry in native conditions (SEC-nMS), was  
140 performed using a BioAccord LC-MS system (Waters, Manchester, UK). The assembly comprises an  
141 Acquity UPLC M-Class system; including a binary solvent manager, a sample manager at 4°C, a column  
142 oven at room temperature, and a UV detector operating at 214 nm and 280 nm, coupled to an RDa  
143 detector. Five µg were injected on a BEH SEC 2.1x150 mm 1.7-µm column (Waters) used with an  
144 isocratic gradient of 150 mM AcNOH<sub>4</sub> (pH 6.9) at a flowrate of 100 mL/min over 6 min. The mass  
145 spectrometer was prior calibrated automatically in the positive mode using the calibration solution  
146 (Waters) and then operated with a capillary voltage of 3.5 kV and a pressure of 2 mbar. The cone  
147 voltage was set to 60V. Acquisitions were performed on the high m/z range 400-7000 with a 1 s scan  
148 time.

149 Data processing was performed using UNIFI v1.913.9 (Waters, Manchester, UK). The avDAR value was  
150 calculated using the equation below:

$$151 \text{ avDAR} = \frac{\sum_{k=0}^n k \times I_k}{\sum_{k=0}^n I_k}$$

152 Where k is the number of drugs and I<sub>k</sub> is the relative peak intensity of DAR<sub>k</sub>.

153 *2.4 Bottom-up peptide mapping analysis*

154 **Sample preparation**—ten µg of the sdADC was solubilized in 150 Mm NH<sub>4</sub>HCO<sub>3</sub> 0.1% RapiGest (Waters)  
155 at pH 7.8, to obtain a final volume of 24 µL. Disulfide reduction was performed by incubation of the  
156 solution with 5 mM DTT for 30 min at 57°C. 10 mM of IAM for 40 min in the dark at room temperature,  
157 was added to alkylate free thiol groups on cysteine residues and prevent reformation of disulfide  
158 bridges.

159 Digestion was performed by adding 5 µL of trypsin solution; *i.e.* 20 µg of trypsin (Promega) suspended  
160 in 100 µL of H<sub>2</sub>O which corresponds to 1:50 enzyme:substrate ratio, at 37°C for 5h. The reaction was  
161 stopped by adding 1% of TFA. RapiGest was eliminated by incubation during 30 min at 37°C and  
162 centrifugation at 13,000 g for 10 min.

163 **LC-MS/MS analysis**—nanoLC-MS/MS analysis was performed using a Dionex Ultimate 3000 LC system.  
164 100 ng of sdADC digest was trapped on a Symmetry C18 pre-column (180 µm x 20 mm, 5 µm particle  
165 size, Waters) and the peptides were separated on an ACQUITY UPLC® BEH130 C18 separation column  
166 (75 µm x 250 mm, 1.7 µm particle size, Waters). The solvent system consisted of 0.1% formic acid in  
167 water (solvent A) and 0.1% formic acid in acetonitrile (solvent B). Peptide trapping was performed  
168 during 3 min at a flow rate of 300 nL/min with 97.5% A and 2.5% B and elution was performed at 40 °C  
169 at a flow rate of 300 nL/min from 7.5% to 50% of B in 37 minutes. For optimal nanoLC-MS/MS, the  
170 mass spectrometer was operated in positive mode, with the following settings: spray voltage 2000 V  
171 and capillary temperature 275°C. The MS scan had a resolution of 120 000, the AGC target was 10<sup>6</sup> and  
172 the maximum IT was 50 ms on m/z [300-1800] range. The MS/MS scans had a resolution of 15 000, the  
173 AGC target was 10<sup>5</sup> and the maximum IT was 22 ms with an Isolation window of 2 m/z. Top 10 HCD  
174 was selected with intensity threshold of 10<sup>4</sup> and dynamic exclusion of 5 s. The normalized collision  
175 energy (NCE) was fixed at 30%. The complete system was fully controlled by Thermo Scientific™  
176 Xcalibur™ software. Raw data collected were processed and converted with MSConvert into .mgf peak  
177 list format.

178 **Data processing**—search engines MASCOT 2.6.2 algorithm (Matrix Science) was used. The search was  
179 performed against the sequence of the light and heavy chains of the ADC. Spectra were searched with  
180 a mass tolerance of 10 ppm for MS and 0.05 Da for MS/MS data. The search was made without enzyme  
181 specified, in order to allow the identification of any non-specific cleavage peptide. Variable  
182 modifications were specified: oxidation of methionine residues, pyro-glutamylation of the N-termini,  
183 deamidation of asparagine, isomerization of aspartic acid residues and drug-linker conjugation (C52 F  
184 H56 N9 O13 and C26 O8 N6 H34) on cysteine residues. Peptide identifications were validated with a  
185 minimal Mascot ion score of 20.

186           2.5 Top-down MS experiments

187 **TD-MS analysis**—a Dionex Ultimate 3000 LC system was used to inject one to 3 µg of samples through  
188 an Agilent Zorbax 300 SB-C8 (2,1 x 50 mm, 1,8 microns) at 60°C. The solvent system consisted of 0.1%  
189 TFA in water (solvent A) and 0.1% TFA in acetonitrile (solvent B). Elution was performed at a flow rate  
190 of 200 µL/min from 20% to 60% of B for 7 minutes. All experiments were performed on an Orbitrap  
191 Tribrid Eclipse MS (Thermo Scientific). The LC was hyphenated to an Orbitrap Tribrid Eclipse MS  
192 (Thermo Scientific) equipped with ETD, HCD and 213 nm UVPD options. For all experiments, the spray  
193 voltage was set to 3.4 kV, and the ion transfer tube temperature at 320 °C.

194 The MS scans were acquired at a resolution of 15 000, the AGC target was 10<sup>6</sup> and the maximum IT at  
195 200 ms on a range of [200-3000] m/z. MS/MS scans had a resolution of 120 000, the AGC target was  
196 10<sup>6</sup> and the maximum IT was 200 ms on m/z [180-2000] with an IW of 2 m/z. The MS scan had a  
197 resolution of 120 000, the normalized AGC target was 250% and the maximum IT was 50 ms on m/z  
198 [300-1800] range. The MS/MS scans had a resolution of 15 000, the nAGC target was 200% and the  
199 maximum IT was 22 ms with an Isolation window of 2 m/z. For HCD fragmentation, the ions were  
200 accelerated under a constant N<sub>2</sub> pressure of 10<sup>-9</sup> mbar with 12 eV. For performing ETD, anionic  
201 fluoranthene radicals were generated in the source region of the instrument. For UVPD, ions were  
202 activated with 213 nm laser delivering a total energy of 150 µJ (2 µJ /pulse).

203 **Data analysis**— the MS/MS spectra were deconvoluted with Xtract algorithm on FreeStyle software,  
204 using a S/N of 3, a fit factor of 70% and a remainder threshold of 25%. The deconvoluted masses were  
205 matched to the protein sequence using ProSight Lite algorithm with a 10-ppm ion tolerance to reduce  
206 the number of false positives. For each fragmentation method the type of the generated ions was  
207 considered, namely b/y in the case of HCD, c/z in the case of ETD, and a/x, b/y and c/z in the case of  
208 UVPD. The C-terminus of the protein was modified with a cysteamination, thus the addition of the  
209 cysteamine mass was considered on this position. Since the addition of the fluorescent AF488 molecule  
210 was targeting the cysteines or the prior added cysteamine, CYS22, CYS96 and the C-terminus was  
211 considered to investigate the specific site of conjugation.

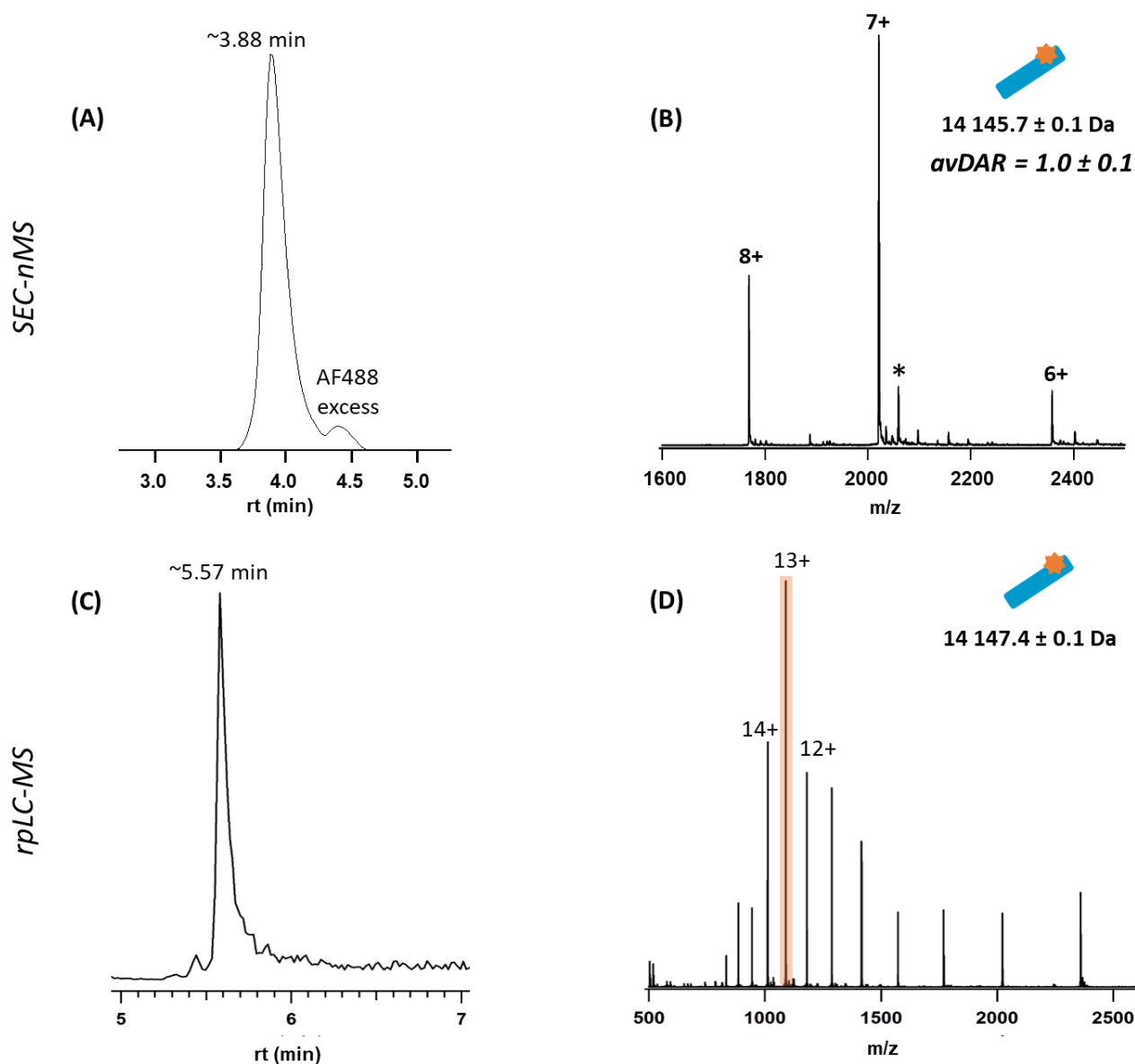
212 To assign the internal fragments, ClipsMS algorithm was used by fixing the parameters as follows:  
213 terminal fragments error at 10 ppm and internal fragments error both at 2 ppm, and smallest internal  
214 fragment size at 2 AA. The cysteamine and AF488 modifications were considered as localized  
215 modifications after confirming their position and type by using ProSight Lite. The fragmentation type  
216 and its corresponding generated ions was considered before starting the search.



217 **3. Results**

218 *3.1 Intact mass analysis using SEC-nMS*

219 Our in-house sdADC was firstly analyzed using SEC-nMS coupling to determine the experimental mass  
220 of the protein, the drug load distribution (DLD), and average drug-to-antibody ratio (avDAR) after  
221 conjugation with the surrogate cytotoxic payload molecule AF488 (**Figure 1A,B**Figure 1). The SEC-UV  
222 chromatogram reveals a major peak at ~3.88 min corresponding to the monomeric sdADC with an  
223 experimental mass of  $14\,145.7 \pm 0.1$  Da that can be assigned to the sdAb conjugated to one AF488  
224 molecule (**Figure 1B**). A minor peak is also observed at ~4.50 min corresponding to a fragmented  
225 moiety of the AF488 (**Figure S2**). According to this result, the conjugation of the sdAb was complete,  
226 leading to an avDAR of 1. This result is in line with the SDS page analysis where the conjugation of the  
227 AF488 molecule was confirmed upon UV visualization of the reduced sdADC (**Figure S3**). However, the  
228 resolution, and mass accuracy of the SEC-nMS coupling allowed to confirm that the experimental mass  
229 of the protein corresponded to the D1 population of the sdADC with a disulfide bridge, suggesting that  
230 the integrity of the intra-molecular linkage between both cysteine residues has been maintained  
231 during the conjugation process.



233

234 **Figure 1:** Analysis of unreduced sdADC in native conditions using SEC-nMS (top panel) and in denaturing conditions using  
 235 rpLC-MS (bottom panel). **(A)** SEC-UV chromatogram. **(B)** MS spectra corresponding to the eluted sdADC in native conditions.  
 236 **(C)** Total ion chromatogram of the reduced sdADC showing one species at ~5.57 min. **(D)** MS spectra of the reduced sdADC  
 237 in denaturing conditions.

238

### 239 3.2 Top-down MS for the sequence characterization and conjugation site identification of 240 the sdADC

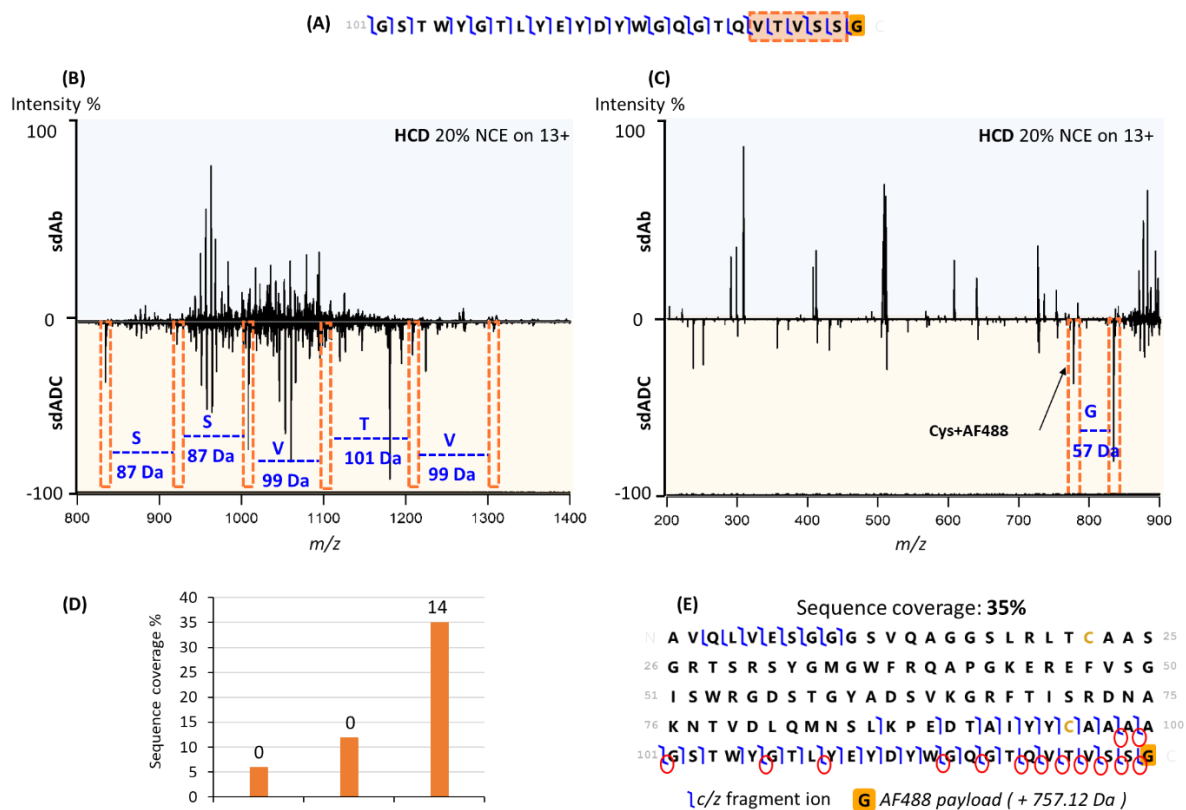
241 Recent studies have shown the benefits of TD-MS for the characterization of protein modifications  
 242 through the direct fragmentation of intact proteins,<sup>27-28, 55-59</sup> although the fragmentation yield is  
 243 significantly reduced when dealing with large molecular ions (> 30 kDa).<sup>34, 42, 60-62</sup> Taking into account  
 244 the relative small size of the sdADC, it seems to be the suitable candidate to be subjected to TD-MS  
 245 workflows in order to perform sequence assessment, along with the localization of the AF488 molecule

246 in the protein backbone. Since the fragmentation yield of the different activation methods diminishes  
247 with the presence of intra-molecular disulfide bonds,<sup>63-65</sup> the conjugation site and the sequence  
248 confirmation of the sdADC were carried out upon reduction of the cysteine residues (see material and  
249 method section, **Figure 1C, D**). The reduction of the disulfide bridge along with the use of chaotropic  
250 agents disrupt the secondary and tertiary structures of the protein, allowing the accommodation of  
251 higher number of protons during the ESI process, and thus increasing the overall net charge state of  
252 the molecular ions. One major peak centered at ~5.57 min is observed in the chromatogram profile of  
253 the sdADC. The charge envelop was centered at the 13+ charge state, and the corresponding  
254 experimental mass associated to the main peak was  $14\ 147.6 \pm 0.2$  Da, in line with the reduced form  
255 of the sdADC bearing one AF488 molecule (+ 757.12 Da) (**Figure 1D**).

256  
257 Subsequently, the reduced sdADC was analyzed using rpLC-TD-MS using different activation  
258 techniques such as HCD, ETD, and UVPD. Optimization of the fragmentation reaction and the charge  
259 state of the precursor molecular ions were conducted on the unconjugated sdAb as a reference sample  
260 (**Figure 1C-D**). Three charge states (12+, 13+ and 14+) were selected for HCD fragmentation combined  
261 with collision energies from 10 to 30 NCE. Interestingly, fragmentation of the 13+ precursor ion gave  
262 rise to the largest number of fragments leading to a sequence coverage of 28% (*versus* 20% and 27%  
263 for 12+ and 14+, respectively, **Figure S4A**). Moreover, the activation energy was also optimized,  
264 reaching 31% of sequence coverage with 20 NCE (**Figure S4B**).

265 The optimized fragmentation conditions were applied to the sdADC. Overall, similar fragmentation  
266 spectra of sdAb, and sdADC were obtained, however, upon pair comparison between both spectra  
267 revealed a series of singly charged fragment ions in the sdADC spectrum that were not detected in the  
268 sdAb fragmentation pattern (**Figure 2B and 2C**) covering the 500-1400 m/z range. Upon calculation of  
269 the mass difference between each consecutive singly-charged ion, it was concluded that those ions  
270 corresponded to the fragmentation of the five last residues of the C-terminal side of the sdADC  
271 (VTVSSG, **Figure 2A**). Additionally, one ion at 776.165 m/z value was observed, corresponding to the  
272 AF488 molecule conjugated to the cysteamine residue. According to these signature ions, the  
273 conjugation of the surrogate cytotoxic payload molecule occurred on the thiol group of the cysteamine  
274 residue located in the C-terminal side of the protein.

275



276

277 **Figure 2:** TD-MS experiments of sdADC. (A) Sequence coverage of the sdADC upon 20% NCE HCD, focused on the C-terminal  
278 region bearing the AF488 modification. (B and C) MS/MS spectra upon 20% NCE HCD fragmentation of sdAb (top) and sdADC  
279 (bottom) showing new fragment ions in the case of the sdADC corresponding to the AF488 modification. (D) Histogram  
280 representing the sequence coverage with the different positions. The numbers on the bars represent the specific fragment  
281 to the modification. (E) Fragmentation map of matched c/z ions with the sdADC sequence. AF488 modification is outlined in  
282 an orange frame. Specific fragments are depicted with red circles

283

284 To further strengthen this result, the variation of the sequence coverage of the sdADC as a function of  
285 the AF488 position was assessed (Figure 2D). Since the conjugations strategy relied on the site selective  
286 maleimide-thiol reaction, the fragment ions were matched with three different sdADC sequences  
287 containing the AF488 molecule at position cys26, cys96, and cysteamine 125. Thus, fragment ion  
288 matching with the conjugation site located at position Cys26, and Cys96 led to a poor sequence  
289 coverage of 6, and 12% respectively with no b-ions containing the aforementioned conjugated cysteine  
290 residues (Figure 2C and S5). Conversely, the sequence coverage rose to 35% when the conjugated  
291 molecule was located at the C-terminal side (cysteamine conjugation), providing 14 diagnostic y-  
292 fragment ions of the position of the AF488 molecule in the cysteamine thiol group (Figure 2D and 2E).  
293 Overall, these results are in line with the singly-charged diagnostic fragments observed upon spectra  
294 comparison between the conjugated and naked sdAb, thus leading to the unambiguous conclusion  
295 that the conjugation of the sdADC was selectively performed in the C-terminal side of the sdADC. This  
296 result was in line with data obtained through peptide mapping analysis. Upon digestion of the sdADC,  
297 only one AF488-bound peptide was found corresponding to the peptide covering the 117-125 region

298 of the protein (**Figure S6**). Combination of TD-MS, and peptide mapping data clearly corroborates the  
 299 selectivity of the bioconjugation strategy used to modify the initial sdAb.

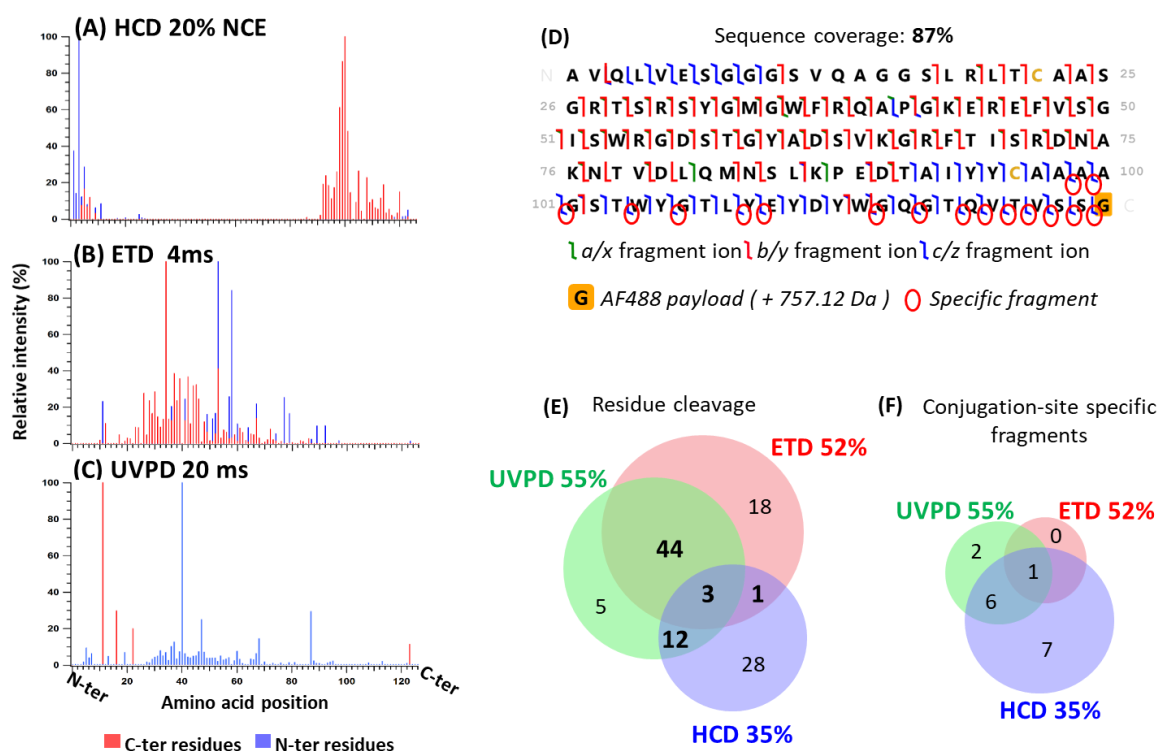
300

301 *Benefits of ETD and UVPD for extended sdADC sequencing*

302 Although the conjugation site is perfectly localized with the sole use of HCD, the fragmentation yield  
 303 remains relatively low for a 14 kDa protein (35%). In order to provide a more extensive sequence  
 304 characterization, the use of complementary activation techniques such as ETD, and UVPD were also  
 305 performed. These two techniques have been shown to provide higher sequence coverage in  
 306 comparison to collision-based fragmentations, covering in a more efficient manner the interior regions  
 307 of protein backbones.<sup>33-34, 36, 39, 66</sup>

308 ETD, and UVPD reaction conditions were chosen from the optimal conditions of the fragmentation of  
 309 the reduced sdAb. Thus, the optimal ETD reaction time was 4 ms whereas 20 ms of irradiation time  
 310 was chosen in the case of UVPD activation. These experimental parameters led to 52%, and 55% of  
 311 sequence coverage of the sdADC, respectively (**Figure S7-S8**), increasing significantly the sequence  
 312 coverage obtained with HCD, as expected.

313



314

315 **Figure 3:** Location of C-terminal and N-terminal residues upon sdADC fragmentation using (A) 20% NCE HCD, (B) 4 ms ETD  
 316 and (C) 20 ms 213 nm UVPD. (D) Total sequence coverage after combination of the three results. AF488 modification is  
 317 outlined in a green frame and specific fragments are depicted in red circles. (E) Residue cleavage of the different  
 318 fragmentation techniques with shared and common fragments. (F) Number of specific fragments to the C-ter modification  
 319 upon HCD, ETD and UVPD.

320

321 According to the ion maps of ETD, and UVPD fragmentations, the mid regions of the sdADC were  
322 efficiently fragmented, especially between the 26, and 76 residues where the sequence coverage was  
323 94%, and 82% for the ETD, and UVPD respectively (**Figure S8C-D**). This region was poorly characterized  
324 with HCD fragmentation), highlighting the great interest of combining orthogonal fragmentation  
325 techniques for an enhanced sequence coverage. Thus, ETD, and UVPD afforded complementary results  
326 in comparison with HCD, with only three fragments shared by the three fragmentation techniques (less  
327 than 2%), raising the overall sdADC sequencing to 87% (**Figure S9**). However, the latter techniques  
328 were not very informative regarding the C-terminal side, and hence the conjugation site of the protein.  
329 ETD only provided with one specific fragment of the conjugation site of the sdADC ( $Z_{11}$ ), and 9  
330 fragments were observed in the case of UVPD. Interestingly, 6 consecutive signature fragment ions  
331 from val121, to gly125 identified in the UVPD spectrum were assigned to  $\gamma$ -type fragment ions that  
332 were not generated during the fragmentation of the sdAb. One possible explanation that could account  
333 for this particular fragmentation behavior could be related with the presence of the AF488 molecule  
334 in the structure of the protein. The chromophore of the AF488 molecule could increase the photon  
335 absorption in the C-terminal side of the protein, favoring the CID-like fragmentation mechanism of the  
336 UVPD in the adjacent residues of the C-terminal site (QVTVSSG). Of note, despite HCD offering the  
337 lowest sequence coverage, it remained the most suitable method to decipher the conjugation site with  
338 14 fragment ions characteristic of the AF488 conjugation at the C-terminal side.

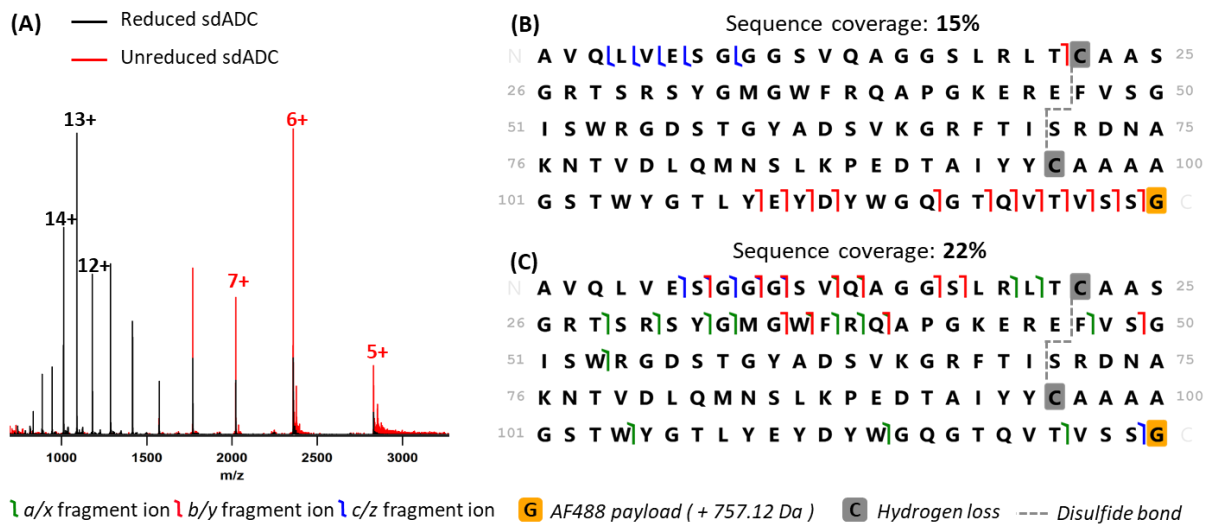
339

#### 340 *TD-MS fragmentation of intact sdADC for direct evidence of intra-molecular disulfide bond preservation*

341 TD-MS strategies have been also applied to proteins with inter,<sup>48, 51, 67-69</sup> and intra-disulfide links.<sup>48, 51,</sup>  
342 <sup>64-65, 68-71</sup> In some cases, different fragmentation techniques were used to disrupt the disulfide bonds  
343 of the proteins with the main purpose of increasing the overall fragmentation yield, and hence provide  
344 a better primary structure characterization. Even though collisional activation techniques can  
345 potentially fragment disulfide bonds,<sup>70-71</sup> electron-driven fragmentation of photo-dissociation  
346 techniques have been shown a more marked propensity to disrupt cysteine-linked proteins either by  
347 promoting a S-S homolytic fragmentation mechanism (accompanied or not by a hydrogen transfer)<sup>67,</sup>  
348 <sup>72</sup> or breaking the C-S bonds.<sup>48, 64, 73</sup> These fragmentation mechanisms give rise to diagnostic fragment  
349 ions that can be capitalized upon, along with the identification of backbone fragments containing  
350 oxidized cysteine residues (H loss modification), not only to increase the overall sequence coverage  
351 but also, to decipher the disulfide patterns of proteins with intra- and inter-molecular disulfide  
352 linkages. Thereby, the different activation methods included in the current study were used to  
353 generate specific fragments of the disulfide bond contained within the structure of the sdADC between

354 the two cysteine residues to provide further evidence about the disulfide linkage integrity upon the  
355 conjugation process.

356 The mass spectrum of the non-reduced sdADC clearly shows a dramatic reduction of the overall charge  
357 state (**Figure 4A**) compared to the mass spectrum of the reduced sample. The charge state distribution  
358 of the reduced sdADC was centered at the 13+ charge state while the most intense species of the non-  
359 reduced sample is the 6+ charge state. This is consistent with the fact that almost 60% of the sdADC  
360 sequence is flanked by the disulfide bond, leading to a more folded structure which precludes the  
361 protonation of the protein, and thus reduces the overall charge state. This characteristic will  
362 presumably impair the fragmentation efficiency of the different fragmentation techniques due to both  
363 the selection of lower charge state precursor ions, and the hindrance for the internal energy  
364 redistribution throughout the whole sdADC sequence. The 6+ charge state precursor ion was isolated  
365 and subjected to the fragmentation with the three activation techniques, *i.e.* HCD, ETD, and UVPD.  
366 Overall, the sequence coverage afforded by the three techniques drastically decreased compared to  
367 the reduced sdADC. HCD, and ETD methods provided fragments on the protein regions that were not  
368 enclosed by the S-S bond, covering the N-, and C-termini of the sdADC with a series of  $\gamma$ -(HCD), and *c*-  
369 ion fragments (ETD) (**Figure 4B and S10-11**). In both cases,  $\gamma$ -, and *c*-ions pinpointed the presence of  
370 both cysteine residues in their oxidized form (*i.e.* involved in the intra-molecular bond). Additionally,  
371 the fragment ions resulting from the HCD activation contained the C-terminal side of the protein  
372 bearing the AF488 molecule, thus simultaneously corroborating the presence of the disulfide bond of  
373 the protein along with the precise conjugation site. In spite of the marked selectivity of ETD  
374 fragmentation to excise disulfide bonds, hallmarks of disulfide bond cleavage could not be found upon  
375 ETD activation. UVPD showed enhanced fragmentation yield, providing 22% of intact sdADC sequence  
376 coverage. In this case, fragment ions in the region enclosed by the disulfide bond were produced,  
377 corresponding to a homolytic S-S cleavage without, in principle, hydrogen transfer (**Figure 4C and S12**).



378

379 **Figure 4:** TD-MS experiments of unreduced sdADC performed on the 6+ charge state precursor ion. **(A)** Comparison of MS  
 380 spectra from rpLC-MS analysis of reduced sdADC (black line) *versus* unreduced sdADC (red line) showing the different charge  
 381 envelopes. **(B)** Fragmentation map upon 10% NCE HCD and 6 ms ETD and **(C)** upon 30 ms 213 nm UVPD. AF488 modification  
 382 is outlined in orange frame and hydrogen loss modifications are in grey frames. The disulfide bond is depicted in grey dashed  
 383 line.

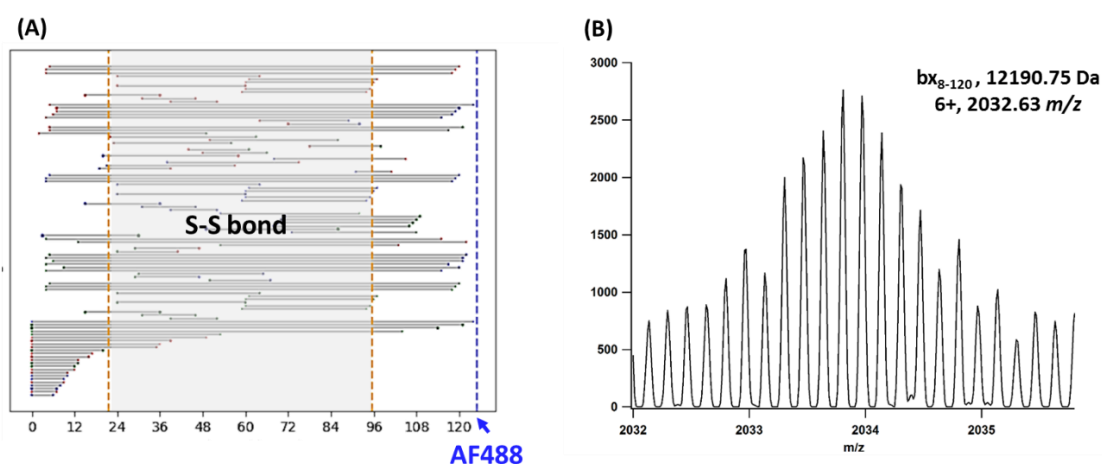
384

385 In order to dig deeper on the identification of produced fragments from the intact sdADC, fragment  
 386 ion search space was extended to internal fragments. Therefore, ClipsMS<sup>74</sup> was used to identify  
 387 fragment ions resulting from multiple protein backbone fragmentation events. The inclusion of  
 388 internal fragments in the ion searching has been shown beneficial in terms of overall sequence  
 389 coverage of cysteine-rich proteins, providing an extensive primary sequence characterization.<sup>41, 65, 70-71</sup>  
 390 In the particular case of the sdADC, these ions were exclusively used to identify fragments ions related  
 391 with the presence of the disulfide bond, *i.e.* either containing both cysteine residues oxidized, or  
 392 fragments resulting from the dissociation of the disulfide bond. After manual validation, no internal  
 393 fragments could be confirmed for HCD, and ETD methods while 10 internal fragments containing the  
 394 intact disulfide bridge could be matched upon UVPD fragmentation (**Figure 5 and S13**) providing more  
 395 specific and straight evidences about the presence of the S-S intra-link. Unfortunately, the triplet  
 396 fragment ion signature (C-S fragmentation) and additional homolytic S-S dissociation were not  
 397 confirmed.

398 One of the reasons that may lead to the absence of disulfide bond cleavage fragment ions identification  
 399 stems from the reduced acquisition time of the MS2 spectra due to the coupling of the LC dimension  
 400 in the forefront of the mass spectrometer. Most of the studies that envisaged the fragmentation of  
 401 intact protein with multiple disulfide bonds are conducted in direct infusion, recording the  
 402 fragmentation spectra during several hundreds of transients.<sup>48, 63-65, 67, 70-72</sup> This is a key parameter that  
 403 facilitates the identification of low abundant ions by increasing the S/N ratio alongside the acquisition  
 404 time. This is even more important for diagnostic fragments characteristics of the disulfide bond



405 fragmentation, which relative intensity has been estimated to be less than 5% of the total fragment  
 406 ion intensity.<sup>63</sup> According to this result, it is highly likely that the reduced acquisition time of the LC-  
 407 TD-MS spectrum of the sdADC (FWHM 0.11 min) precludes the detection of these low-abundant  
 408 fragment ions. However, the results recorded with the three fragmentation techniques clearly  
 409 demonstrate the connectivity of the S-S bond from the Cys22 to the Cys96 residues after confirming  
 410 the presence of terminal and internal fragments containing both oxidized cysteine residues. The  
 411 contribution of both types of ions clearly led to the confirmation of disulfide linkage of both cysteine  
 412 residues, and thus providing a more comprehensive characterization of the nanobody structure.  
 413



414  
 415 **Figure 5:** Added value of internal fragments consideration for the identification of the disulfide bond on the unreduced form  
 416 of the sdADC. **(A)** Fragments location map upon 30 ms UVPD. Orange dashed lines represent the position of the cysteines  
 417 involved in the S-S bond and blue dashed line represent the position of the AF488 modification. **(B)** Isotopic profile of an  
 418 internal fragment (*bx<sub>8-120</sub>*) bearing both cysteines involved in the S-S bond.  
 419

#### 420 4. Conclusions

421 The current study reports for the first time on the characterization of a sdADC conjugated with a  
 422 surrogate cytotoxic payload molecule using an optimized LC-TD-MS workflow based on three different  
 423 activation techniques, *i.e.* HCD, ETD, and UVPD. The results clearly highlight the benefits and  
 424 limitations of all the three techniques in terms of sequence coverage, conjugation site, and  
 425 determination/fragmentation of intramolecular disulfide bonds in order to afford the most  
 426 comprehensive characterization of the sdADC primary structure.

427 Upon unveiling the number of conjugated molecules attached to the sdAb sequence, the conjugated  
 428 protein was interrogated with the three different activation methods. As expected by previous  
 429 analyses, ETD, and UVPD provided extensive sequence characterization, especially in the mid-region  
 430 of the sdADC. However, HCD fragmentation was more informative regarding the number of fragment  
 431 ions that were diagnostic to the specific conjugation site. This result seems to disagree with previous

432 studies where electron- and photo-dissociation techniques outperformed the results of collisional  
433 activation techniques.<sup>34-36</sup> Two main reasons can account for this observation. The first one is that the  
434 conjugation site of the sdADC is located in the C-terminal extremity, a region which is normally well  
435 sequenced by collisional activation techniques. The second one is that the structure of the cargo  
436 molecule used in this study does not contain an ester bond that is commonly used to covalently attach  
437 the cytotoxic molecule to the linker of more classical ADC payloads. As a consequence, the AF488  
438 moiety exhibits more resistance to undergo fragmentation, and thus remaining intact upon collisions  
439 with the background gas.

440 The LC-TD-MS workflow was also applied to the non-reduced sdADC sample to determine the presence  
441 of the intramolecular S-S bond after conjugation of the AF488 molecule. The fragmentation efficiency  
442 of the three techniques drastically decreased since the disulfide bond stabilizes the secondary  
443 structure of the protein leading to a more compact, and less charged entity. The overall sequence  
444 coverage upon combination of the three techniques led to a final 33%. Only a limited number of  
445 fragment ions characteristics of the disulfide bond cleavage were identified upon UVPD fragmentation.  
446 This is in good agreement with previous studies showing that UVPD is less sensitive to the net charge  
447 state of the precursor ion,<sup>75-76</sup> and affords a marked propensity to fragment disulfide bonds.<sup>67, 77</sup> The  
448 vast majority of fragment ions stemmed from the fragmentation of the regions near the N-, and C-  
449 termini that were not encompassed by the intra-molecular bond. Nevertheless, these ions (either  
450 terminal or internal ions) corroborated the presence of the disulfide bridge along with the localization  
451 of the AF488 molecule in the C-terminal side.

452 Altogether, these results put in evidence that despite the relatively low molecular weight, and the  
453 limited structural heterogeneity, the fragmentation and comprehensive characterization of sdAb, and  
454 sdADCs at the intact level is still challenge, especially when TD-MS experimental workflows are  
455 conducted in the chromatography time scale. However, the use of complementary activation  
456 techniques, and tailored fragment ion searches can boost the performances of these workflows in  
457 terms of sequence coverage and signature fragment ions, spurring their application to the  
458 characterization of a large array of proteins.

## 459 5. References

- 460 1. Crescioli, S.,Kaplun, H.,Chenoweth, A.,Wang, L.,Visweswaraiah, J.,Reichert, J. M.: Antibodies to watch in  
461 2024. *MAbs* 16 (1), 2297450 (2024).
- 462 2. Jin, B. K.,Odongo, S.,Radwanska, M.,Magez, S.: Nanobodies: A Review of Generation, Diagnostics and  
463 Therapeutics. *International journal of molecular sciences* 24 (6), (2023).
- 464 3. Yong Joon Kim, J.,Sang, Z.,Xiang, Y.,Shen, Z.,Shi, Y.: Nanobodies: Robust miniprotein binders in  
465 biomedicine. *Advanced drug delivery reviews* 195 114726 (2023).
- 466 4. Hamers-Casterman, C.,Atarhouch, T.,Muyldermans, S.,Robinson, G.,Hammers, C.,Songa, E.  
467 B.,Bendahman, N.,Hammers, R.: Naturally occurring antibodies devoid of light chains. *Nature* 363 (6428), 446-448  
468 (1993).

469 5. Greenberg, A. S.,Avila, D.,Hughes, M.,Hughes, A.,McKinney, E. C.,Flajnik, M. F.: A new antigen receptor  
470 gene family that undergoes rearrangement and extensive somatic diversification in sharks. *Nature* 374 (6518), 168-  
471 173 (1995).

472 6. Kijanka, M.,Dorresteijn, B.,Oliveira, S.,van Bergen en Henegouwen, P. M.: Nanobody-based cancer  
473 therapy of solid tumors. *Nanomedicine (London, England)* 10 (1), 161-74 (2015).

474 7. Wang, L.,Zhang, G.,Qin, L.,Ye, H.,Wang, Y.,Long, B.,Jiao, Z.: Anti-EGFR Binding Nanobody Delivery  
475 System to Improve the Diagnosis and Treatment of Solid Tumours. *Recent patents on anti-cancer drug discovery*  
476 15 (3), 200-211 (2020).

477 8. Bélanger, K.,Iqbal, U.,Tanha, J.,MacKenzie, R.,Moreno, M.,Stanimirovic, D.: Single-Domain Antibodies as  
478 Therapeutic and Imaging Agents for the Treatment of CNS Diseases. *Antibodies (Basel, Switzerland)* 8 (2), (2019).

479 9. Pothin, E.,Lesuisse, D.,Lafaye, P.: Brain Delivery of Single-Domain Antibodies: A Focus on VHH and  
480 VNAR. *Pharmaceutics* 12 (10), (2020).

481 10. Henry, K. A.,MacKenzie, C. R.: Antigen recognition by single-domain antibodies: structural latitudes and  
482 constraints. *MAbs* 10 (6), 815-826 (2018).

483 11. De Genst, E.,Silence, K.,Decanniere, K.,Conrath, K.,Loris, R.,Kinne, J.,Muyldermans, S.,Wyns, L.:  
484 Molecular basis for the preferential cleft recognition by dromedary heavy-chain antibodies. *Proc Natl Acad Sci U S*  
485 *A* 103 (12), 4586-91 (2006).

486 12. Ackaert, C.,Smiejkowska, N.,Xavier, C.,Sterckx, Y. G. J.,Denies, S.,Stijlemans, B.,Elkrim, Y.,Devoogdt,  
487 N.,Caveliers, V.,Lahoutte, T.,Muyldermans, S.,Breckpot, K.,Keyaerts, M.: Immunogenicity Risk Profile of  
488 Nanobodies. *Frontiers in immunology* 12 632687 (2021).

489 13. Rossotti, M. A.,Bélanger, K.,Henry, K. A.,Tanha, J.: Immunogenicity and humanization of single-domain  
490 antibodies. *The FEBS journal* 289 (14), 4304-4327 (2022).

491 14. Wang, Y.,Fan, Z.,Shao, L.,Kong, X.,Hou, X.,Tian, D.,Sun, Y.,Xiao, Y.,Yu, L.: Nanobody-derived  
492 nanobiotechnology tool kits for diverse biomedical and biotechnology applications. *International journal of*  
493 *nanomedicine* 11 3287-303 (2016).

494 15. Dumoulin, M.,Conrath, K.,Van Meirhaeghe, A.,Meersman, F.,Heremans, K.,Frenken, L. G.,Muyldermans,  
495 S.,Wyns, L.,Matagne, A.: Single-domain antibody fragments with high conformational stability. *Protein Sci.* 11 (3),  
496 500-15 (2002).

497 16. Ruano-Gallego, D.,Fraile, S.,Gutierrez, C.,Fernández, L. Á.: Screening and purification of nanobodies from  
498 *E. coli* culture supernatants using the hemolysin secretion system. *Microbial Cell Factories* 18 (1), 47 (2019).

499 17. Gorlani, A.,de Haard, H.,Verrips, T.: Expression of VHHs in *Saccharomyces cerevisiae*. *Methods in*  
500 *molecular biology (Clifton, N.J.)* 911 277-86 (2012).

501 18. Mei, Y.,Chen, Y.,Sivaccumar, J. P.,An, Z.,Xia, N.,Luo, W.: Research progress and applications of  
502 nanobody in human infectious diseases. *Frontiers in pharmacology* 13 963978 (2022).

503 19. Liu, M.,Li, L.,Jin, D.,Liu, Y.: Nanobody-A versatile tool for cancer diagnosis and therapeutics. *Wiley*  
504 *interdisciplinary reviews. Nanomedicine and nanobiotechnology* 13 (4), e1697 (2021).

505 20. Gao, Y.,Zhu, J.,Lu, H.: Single domain antibody-based vectors in the delivery of biologics across the blood-  
506 brain barrier: a review. *Drug delivery and translational research* 11 (5), 1818-1828 (2021).

507 21. Pronk, S. D.,Schooten, E.,Heinen, J.,Helfrich, E.,Oliveira, S.,van Bergen En Henegouwen, P. M. P.: Single  
508 Domain Antibodies as Carriers for Intracellular Drug Delivery: A Proof of Principle Study. *Biomolecules* 11 (7),  
509 (2021).

510 22. Barakat, S.,Berksoz, M.,Zahedimaram, P.,Piepoli, S.,Erman, B.: Nanobodies as molecular imaging  
511 probes. *Free radical biology & medicine* 182 260-275 (2022).

512 23. Brown, K. A.,Tucholski, T.,Alpert, A. J.,Eken, C.,Wesemann, L.,Kyrvasilis, A.,Jin, S.,Ge, Y.: Top-Down  
513 Proteomics of Endogenous Membrane Proteins Enabled by Cloud Point Enrichment and Multidimensional Liquid  
514 Chromatography-Mass Spectrometry. *Anal. Chem.* 92 (24), 15726-15735 (2020).

515 24. Juliano, B. R.,Keating, J. W.,Ruotolo, B. T.: Infrared Photoactivation Enables Improved Native Top-Down  
516 Mass Spectrometry of Transmembrane Proteins. *Anal. Chem.* 95 (35), 13361-13367 (2023).

517 25. Lutomski, C. A.,El-Baba, T. J.,Hinkle, J. D.,Liko, I.,Bennett, J. L.,Kalmankar, N. V.,Dolan, A.,Kirschbaum,  
518 C.,Greis, K.,Urner, L. H.,Kapoor, P.,Yen, H. Y.,Pagel, K.,Mullen, C.,Syka, J. E. P.,Robinson, C. V.: Infrared  
519 Multiphoton Dissociation Enables Top-Down Characterization of Membrane Protein Complexes and G Protein-  
520 Coupled Receptors. *Angew. Chem. Int. Ed. Engl.* 62 (36), e202305694 (2023).

521 26. Gault, J.,Liko, I.,Landreh, M.,Shutin, D.,Bolla, J. R.,Jefferies, D.,Agasid, M.,Yen, H. Y.,Ladds, M.,Lane, D.  
522 P.,Khalid, S.,Mullen, C.,Remes, P. M.,Huguet, R.,McAlister, G.,Goodwin, M.,Viner, R.,Syka, J. E. P.,Robinson, C.  
523 V.: Combining native and 'omics' mass spectrometry to identify endogenous ligands bound to membrane proteins.  
524 *Nat Methods* 17 (5), 505-508 (2020).

525 27. Walker, J. N.,Lam, R.,Brodbeck, J. S.: Enhanced Characterization of Histones Using 193 nm Ultraviolet  
526 Photodissociation and Proton Transfer Charge Reduction. *Anal. Chem.* 95 (14), 5985-5993 (2023).

527 28. Berthias, F.,Thurman, H. A.,Wijegunawardena, G.,Wu, H.,Shvartsburg, A. A.,Jensen, O. N.: Top-Down Ion  
528 Mobility Separations of Isomeric Proteoforms. *Anal. Chem.* 95 (2), 784-791 (2023).

529 29. Jeanne Dit Fouque, K.,Miller, S. A.,Pham, K.,Bhanu, N. V.,Cintron-Diaz, Y. L.,Leyva, D.,Kaplan, D.,Voinov,  
530 V. G.,Ridgeway, M. E.,Park, M. A.,Garcia, B. A.,Fernandez-Lima, F.: Top-"Double-Down" Mass Spectrometry of  
531 Histone H4 Proteoforms: Tandem Ultraviolet-Photon and Mobility/Mass-Selected Electron Capture Dissociations.  
532 *Anal. Chem.* 94 (44), 15377-15385 (2022).

533 30. Peters-Clarke, T. M.,Quan, Q.,Brademan, D. R.,Hebert, A. S.,Westphall, M. S.,Coon, J. J.: Ribonucleic  
534 Acid Sequence Characterization by Negative Electron Transfer Dissociation Mass Spectrometry. *Anal. Chem.* 92  
535 (6), 4436-4444 (2020).

536 31. Santos, I. C.,Lanzillotti, M.,Shilov, I.,Basanta-Sanchez, M.,Roushan, A.,Lawler, R.,Tang, W.,Bern,  
537 M.,Brodbeck, J. S.: Ultraviolet Photodissociation and Activated Electron Photodetachment Mass Spectrometry for  
538 Top-Down Sequencing of Modified Oligoribonucleotides. *J. Am. Soc. Mass. Spectrom.* 33 (3), 510-520 (2022).

539 32. Crittenden, C. M.,Lanzillotti, M. B.,Chen, B.: Top-Down Mass Spectrometry of Synthetic Single Guide  
540 Ribonucleic Acids Enabled by Facile Sample Clean-Up. *Anal. Chem.* 95 (6), 3180-3186 (2023).

541 33. Dhenin, J.,Dupré, M.,Druart, K.,Krick, A.,Mauriac, C.,Chamot-Rooke, J.: A multiparameter optimization in  
542 middle-down analysis of monoclonal antibodies by LC-MS/MS. *J. Mass Spectrom.* 58 (3), e4909 (2023).

543 34. Beaumal, C.,Deslignière, E.,Diemer, H.,Carapito, C.,Cianféroni, S.,Hernandez-Alba, O.: Improved  
544 characterization of trastuzumab deruxtecan with PTCL and internal fragments implemented in middle-down MS  
545 workflows. *Anal Bioanal Chem* (2023).

546 35. Watts, E.,Williams, J. D.,Miesbauer, L. J.,Bruncko, M.,Brodbeck, J. S.: Comprehensive Middle-Down Mass  
547 Spectrometry Characterization of an Antibody-Drug Conjugate by Combined Ion Activation Methods. *Anal. Chem.*  
548 92 (14), 9790-9798 (2020).

549 36. Hernandez-Alba, O.,Houel, S.,Hessmann, S.,Erb, S.,Rabuka, D.,Huguet, R.,Josephs, J.,Beck, A.,Drake,  
550 P. M.,Cianféroni, S.: A Case Study to Identify the Drug Conjugation Site of a Site-Specific Antibody-Drug-Conjugate  
551 Using Middle-Down Mass Spectrometry. *J. Am. Soc. Mass. Spectrom.* 30 (11), 2419-2429 (2019).

552 37. Chen, B.,Lin, Z.,Zhu, Y.,Jin, Y.,Larson, E.,Xu, Q.,Fu, C.,Zhang, Z.,Zhang, Q.,Pritts, W. A.,Ge, Y.: Middle-  
553 Down Multi-Attribute Analysis of Antibody-Drug Conjugates with Electron Transfer Dissociation. *Anal. Chem.* 91  
554 (18), 11661-11669 (2019).

555 38. Srzentic, K.,Nagornov, K. O.,Fornelli, L.,Lobas, A. A.,Ayoub, D.,Kozhinov, A. N.,Gasilova, N.,Menin,  
556 L.,Beck, A.,Gorshkov, M. V.,Aizikov, K.,Tsybin, Y. O.: Multiplexed Middle-Down Mass Spectrometry as a Method  
557 for Revealing Light and Heavy Chain Connectivity in a Monoclonal Antibody. *Anal. Chem.* 90 (21), 12527-12535  
558 (2018).

559 39. Cotham, V. C.,Brodbeck, J. S.: Characterization of Therapeutic Monoclonal Antibodies at the Subunit-Level  
560 using Middle-Down 193 nm Ultraviolet Photodissociation. *Anal. Chem.* 88 (7), 4004-4013 (2016).

561 40. Fornelli, L.,Ayoub, D.,Aizikov, K.,Beck, A.,Tsybin, Y. O.: Middle-Down Analysis of Monoclonal Antibodies  
562 with Electron Transfer Dissociation Orbitrap Fourier Transform Mass Spectrometry. *Anal. Chem.* 86 (6), 3005-3012  
563 (2014).

564 41. Wei, B.,Lantz, C.,Ogorzalek Loo, R. R.,Campuzano, I. D. G.,Loo, J. A.: Internal Fragments Enhance  
565 Middle-Down Mass Spectrometry Structural Characterization of Monoclonal Antibodies and Antibody-Drug  
566 Conjugates. *Anal. Chem.* (2024).

567 42. Melani, R. D.,Srzentić, K.,Gerbasi, V. R.,McGee, J. P.,Huguet, R.,Fornelli, L.,Kelleher, N. L.: Direct  
568 measurement of light and heavy antibody chains using ion mobility and middle-down mass spectrometry. *MAbs* 11  
569 (8), 1351-1357 (2019).

570 43. Fornelli, L.,Damoc, E.,Thomas, P. M.,Kelleher, N. L.,Aizikov, K.,Denisov, E.,Makarov, A.,Tsybin, Y. O.:  
571 Analysis of Intact Monoclonal Antibody IgG1 by Electron Transfer Dissociation Orbitrap FTMS. *Molecular & Cellular*  
572 *Proteomics* 11 (12), 1758-1767 (2012).

573 44. Tsybin, Y. O.,Fornelli, L.,Stoermer, C.,Luebeck, M.,Parra, J.,Nallet, S.,Wurm, F. M.,Hartmer, R.: Structural  
574 Analysis of Intact Monoclonal Antibodies by Electron Transfer Dissociation Mass Spectrometry. *Anal. Chem.* 83  
575 (23), 8919-8927 (2011).

576 45. Fornelli, L.,Ayoub, D.,Aizikov, K.,Liu, X.,Damoc, E.,Pevzner, P. A.,Makarov, A.,Beck, A.,Tsybin, Y. O.:  
577 Top-down analysis of immunoglobulin G isotypes 1 and 2 with electron transfer dissociation on a high-field Orbitrap  
578 mass spectrometer. *Journal of proteomics* 159 67-76 (2017).

579 46. Mao, Y.,Valeja, S. G.,Rouse, J. C.,Hendrickson, C. L.,Marshall, A. G.: Top-Down Structural Analysis of an  
580 Intact Monoclonal Antibody by Electron Capture Dissociation-Fourier Transform Ion Cyclotron Resonance-Mass  
581 Spectrometry. *Anal. Chem.* 85 (9), 4239-4246 (2013).

582 47. Lodge, J. M.,Schauer, K. L.,Brademan, D. R.,Riley, N. M.,Shishkova, E.,Westphall, M. S.,Coon, J. J.: Top-  
583 Down Characterization of an Intact Monoclonal Antibody Using Activated Ion Electron Transfer Dissociation. *Anal.*  
584 *Chem.* 92 (15), 10246-10251 (2020).

585 48. Shaw, J. B.,Liu, W.,Vasil Ev, Y. V.,Bracken, C. C.,Malhan, N.,Guthals, A.,Beckman, J. S.,Voinov, V. G.:  
586 Direct Determination of Antibody Chain Pairing by Top-down and Middle-down Mass Spectrometry Using Electron  
587 Capture Dissociation and Ultraviolet Photodissociation. *Anal. Chem.* 92 (1), 766-773 (2020).

588 49. Srzentić, K.,Fornelli, L.,Tsybin, Y. O.,Loo, J. A.,Seckler, H.,Agar, J. N.,Anderson, L. C.,Bai, D. L.,Beck,  
589 A.,Brodbeck, J. S.,van der Burgt, Y. E. M.,Chamot-Rooke, J.,Chatterjee, S.,Chen, Y.,Clarke, D. J.,Danis, P.  
590 O.,Diedrich, J. K.,D'Ippolito, R. A.,Dupré, M.,Gasilova, N.,Ge, Y.,Goo, Y. A.,Goodlett, D. R.,Greer, S.,Haselmann,  
591 K. F.,He, L.,Hendrickson, C. L.,Hinkle, J. D.,Holt, M. V.,Hughes, S.,Hunt, D. F.,Kelleher, N. L.,Kozhinov, A. N.,Lin,  
592 Z.,Malosse, C.,Marshall, A. G.,Menin, L.,Millikin, R. J.,Nagornov, K. O.,Nicolardi, S.,Paša-Tolić, L.,Pengelley,  
593 S.,Quebbemann, N. R.,Resemann, A.,Sandoval, W.,Sarin, R.,Schmitt, N. D.,Shabanowitz, J.,Shaw, J.  
594 B.,Shortreed, M. R.,Smith, L. M.,Sobott, F.,Suckau, D.,Toby, T.,Weisbrod, C. R.,Wildburger, N. C.,Yates, J. R.,  
595 3rd,Yoon, S. H.,Young, N. L.,Zhou, M.: Interlaboratory Study for Characterizing Monoclonal Antibodies by Top-  
596 Down and Middle-Down Mass Spectrometry. *J. Am. Soc. Mass. Spectrom.* 31 (9), 1783-1802 (2020).

597 50. Fornelli, L.,Srzentić, K.,Huguet, R.,Mullen, S.,Sharma, S.,Zabrouskov, V.,Fellers, R. T.,Durbin, K.  
598 R.,Compton, P. D.,Kelleher, N. L.: Accurate Sequence Analysis of a Monoclonal Antibody by Top-Down and Middle-  
599 Down Orbitrap Mass Spectrometry Applying Multiple Ion Activation Techniques. *Anal. Chem.* 90 (14), 8421-8429  
600 (2018).

601 51. Wei, B.,Lantz, C.,Liu, W.,Viner, R.,Ogorzalek Loo, R. R.,Campuzano, I. D. G.,Loo, J. A.: Added Value of  
602 Internal Fragments for Top-Down Mass Spectrometry of Intact Monoclonal Antibodies and Antibody-Drug  
603 Conjugates. *Anal. Chem.* (2023).

604 52. Larson, E. J.,Roberts, D. S.,Melby, J. A.,Buck, K. M.,Zhu, Y.,Zhou, S.,Han, L.,Zhang, Q.,Ge, Y.: High-  
605 Throughput Multi-attribute Analysis of Antibody-Drug Conjugates Enabled by Trapped Ion Mobility Spectrometry  
606 and Top-Down Mass Spectrometry. *Anal. Chem.* 93 (29), 10013-10021 (2021).

607 53. Resemann, A.,Wunderlich, D.,Rothbauer, U.,Warscheid, B.,Leonhardt, H.,Fuchser, J.,Kuhlmann,  
608 K.,Suckau, D.: Top-down de Novo protein sequencing of a 13.6 kDa camelid single heavy chain antibody by matrix-  
609 assisted laser desorption ionization-time-of-flight/time-of-flight mass spectrometry. *Anal. Chem.* 82 (8), 3283-92  
610 (2010).

611 54. Macias, L. A.,Wang, X.,Davies, B. W.,Brodbeck, J. S.: Mapping paratopes of nanobodies using native mass  
612 spectrometry and ultraviolet photodissociation. *Chem Sci* 13 (22), 6610-6618 (2022).

613 55. Rogers, H. T.,Roberts, D. S.,Larson, E. J.,Melby, J. A.,Rossler, K. J.,Carr, A. V.,Brown, K. A.,Ge, Y.:  
614 Comprehensive Characterization of Endogenous Phospholamban Proteoforms Enabled by Photocleavable  
615 Surfactant and Top-down Proteomics. *Anal. Chem.* 95 (35), 13091-13100 (2023).

616 56. Dunham, S. D.,Wei, B.,Lantz, C.,Loo, J. A.,Brodbeck, J. S.: Impact of Internal Fragments on Top-Down  
617 Analysis of Intact Proteins by 193 nm UVPD. *J Proteome Res* 22 (1), 170-181 (2023).

618 57. Brodbelt, J. S.: Deciphering combinatorial post-translational modifications by top-down mass spectrometry.  
619 *Curr. Opin. Chem. Biol.* 70 102180 (2022).

620 58. Greer, S. M.,Brodbeck, J. S.: Top-Down Characterization of Heavily Modified Histones Using 193 nm  
621 Ultraviolet Photodissociation Mass Spectrometry. *J Proteome Res* 17 (3), 1138-1145 (2018).

622 59. Miller, S. A.,Jeanne Dit Fouque, K.,Hard, E. R.,Balana, A. T.,Kaplan, D.,Voinov, V. G.,Ridgeway, M.  
623 E.,Park, M. A.,Anderson, G. A.,Pratt, M. R.,Fernandez-Lima, F.: Top/Middle-Down Characterization of  $\alpha$ -Synuclein  
624 Glycoforms. *Anal. Chem.* 95 (49), 18039-18045 (2023).

625 60. Fornelli, L.,Parra, J.,Hartmer, R.,Stoermer, C.,Lubeck, M.,Tsybin, Y. O.: Top-down analysis of 30-80 kDa  
626 proteins by electron transfer dissociation time-of-flight mass spectrometry. *Analytical and Bioanalytical Chemistry*  
627 405 (26), 8505-8514 (2013).

628 61. Kline, J. T.,Mullen, C.,Durbin, K. R.,Oates, R. N.,Huguet, R.,Syka, J. E. P.,Fornelli, L.: Sequential Ion-Ion  
629 Reactions for Enhanced Gas-Phase Sequencing of Large Intact Proteins in a Tribrid Orbitrap Mass Spectrometer.  
630 *J. Am. Soc. Mass. Spectrom.* 32 (9), 2334-2345 (2021).

631 62. Fornelli, L.,Sržentić, K.,Huguet, R.,Mullen, C.,Sharma, S.,Zabrouskov, V.,Fellers, R. T.,Durbin, K.  
632 R.,Compton, P. D.,Kelleher, N. L.: Accurate Sequence Analysis of a Monoclonal Antibody by Top-Down and Middle-  
633 Down Orbitrap Mass Spectrometry Applying Multiple Ion Activation Techniques. *Anal. Chem.* 90 (14), 8421-8429  
634 (2018).

635 63. Zhang, J.,Ogorzalek Loo, R. R.,Loo, J. A.: Increasing Fragmentation of Disulfide-Bonded Proteins for Top-  
636 Down Mass Spectrometry by Supercharging. *Int. J. Mass spectrom.* 377 546-556 (2015).

637 64. Rush, M. J. P.,Riley, N. M.,Westphall, M. S.,Coon, J. J.: Top-Down Characterization of Proteins with Intact  
638 Disulfide Bonds Using Activated-Ion Electron Transfer Dissociation. *Anal. Chem.* 90 (15), 8946-8953 (2018).

639 65. Wei, B.,Zenaidee, M. A.,Lantz, C.,Williams, B. J.,Totten, S.,Ogorzalek Loo, R. R.,Loo, J. A.: Top-down  
640 mass spectrometry and assigning internal fragments for determining disulfide bond positions in proteins. *Analyst*  
641 148 (1), 26-37 (2022).

642 66. Juetten, K. J.,Brodbeck, J. S.: Top-Down Analysis of Supercharged Proteins Using Collision-, Electron-,  
643 and Photon-Based Activation Methods. *J. Am. Soc. Mass. Spectrom.* 34 (7), 1467-1476 (2023).

644 67. Macias, L. A.,Brodbeck, J. S.: Investigation of Product Ions Generated by 193 nm Ultraviolet  
645 Photodissociation of Peptides and Proteins Containing Disulfide Bonds. *J. Am. Soc. Mass. Spectrom.* 33 (7), 1315-  
646 1324 (2022).

647 68. Gammelgaard, S. K.,Petersen, S. B.,Haselmann, K. F.,Nielsen, P. K.: Characterization of Insulin Dimers  
648 by Top-Down Mass Spectrometry. *J. Am. Soc. Mass. Spectrom.* 32 (8), 1910-1918 (2021).

649 69. Quick, M. M.,Crittenden, C. M.,Rosenberg, J. A.,Brodbeck, J. S.: Characterization of Disulfide Linkages in  
650 Proteins by 193 nm Ultraviolet Photodissociation (UVPD) Mass Spectrometry. *Anal. Chem.* 90 (14), 8523-8530  
651 (2018).

652 70. Chen, J.,Shiyanov, P.,Zhang, L.,Schlager, J. J.,Green-Church, K. B.: Top-down characterization of a  
653 native highly intralinked protein: concurrent cleavages of disulfide and protein backbone bonds. *Anal. Chem.* 82  
654 (14), 6079-89 (2010).

655 71. Chen, J.,Shiyanov, P.,Schlager, J. J.,Green, K. B.: A pseudo MS3 approach for identification of disulfide-  
656 bonded proteins: uncommon product ions and database search. *J. Am. Soc. Mass. Spectrom.* 23 (2), 225-43 (2012).

657 72. Zhao, X.,Shen, Y.,Tong, W.,Wang, G.,Chen, D. Y.: Deducing disulfide patterns of cysteine-rich proteins  
658 using signature fragments produced by top-down mass spectrometry. *Analyst* 143 (4), 817-823 (2018).

659 73. Sržentić, K.,Nagornov, K. O.,Fornelli, L.,Lobas, A. A.,Ayoub, D.,Kozhinov, A. N.,Gasilova, N.,Menin,  
660 L.,Beck, A.,Gorshkov, M. V.,Aizikov, K.,Tsybin, Y. O.: Multiplexed Middle-Down Mass Spectrometry as a Method  
661 for Revealing Light and Heavy Chain Connectivity in a Monoclonal Antibody. *Anal. Chem.* 90 (21), 12527-12535  
662 (2018).

663 74. Lantz, C.,Zenaidee, M. A.,Wei, B.,Hemming, Z.,Ogorzalek Loo, R. R.,Loo, J. A.: ClipsMS: An Algorithm  
664 for Analyzing Internal Fragments Resulting from Top-Down Mass Spectrometry. *J Proteome Res* 20 (4), 1928-1935  
665 (2021).

666 75. Bashyal, A.,Sanders, J. D.,Holden, D. D.,Brodbeck, J. S.: Top-Down Analysis of Proteins in Low Charge  
667 States. *J. Am. Soc. Mass. Spectrom.* 30 (4), 704-717 (2019).

- 668 76. Brodbelt, J. S., Morrison, L. J., Santos, I.: Ultraviolet Photodissociation Mass Spectrometry for Analysis of  
669 Biological Molecules. *Chem. Rev.* 120 (7), 3328-3380 (2020).  
670 77. Talbert, L. E., Julian, R. R.: Directed-Backbone Dissociation Following Bond-Specific Carbon-Sulfur UVPD  
671 at 213 nm. *J. Am. Soc. Mass. Spectrom.* 29 (9), 1760-1767 (2018).  
672